

NASA Contractor Report 178212

ICASE REPORT NO. 86-81

ICASE

ANALYSIS OF THE SOR ITERATION FOR THE 9-POINT LAPLACIAN

Loyce M. Adams

Randall J. LeVeque

David M. Young

Contract No. NAS1-18107

December 1986

(NASA-CR-178212) ANALYSIS OF THE SOR
ITERATION FOR THE 9-POINT LAPLACIAN Final
Report (NASA) 40 p CSCL 12A

N87-16552

Unclas

G3/64 43310

INSTITUTE FOR COMPUTER APPLICATIONS IN SCIENCE AND ENGINEERING
NASA Langley Research Center, Hampton, Virginia 23665

Operated by the Universities Space Research Association



National Aeronautics and
Space Administration

Langley Research Center
Hampton, Virginia 23665

ANALYSIS OF THE SOR ITERATION FOR THE 9-POINT LAPLACIAN

Loyce M. Adams⁺
University of Washington

Randall J. LeVeque⁺⁺
University of Washington

David M. Young^{*}
University of Texas at Austin

ABSTRACTS

The SOR iteration for solving linear systems of equations depends upon an overrelaxation factor ω . A theory for determining ω was given by Young [1950] for consistently ordered matrices. Here we determine the optimal ω for the 9-point stencil for the model problem of Laplace's equation on a square. We consider several orderings of the equations, including the natural rowwise and multicolor orderings, all of which lead to non-consistently ordered matrices, and find two equivalence classes of orderings with different convergence behavior and optimal ω 's. We compare our results for the natural rowwise ordering to those of Garabedian [1956] and explain why both results are, in a sense, correct, even though they differ. We also analyze a pseudo SOR method for the model problem and show that it is not as effective as the SOR methods. Finally, we compare the point SOR methods to known results for line SOR methods for this problem.

This research was supported in part by NASA Contract NAS1-18107 while the first and second authors were in residence at the Institute for Computer Applications in Science and Engineering (ICASE), NASA Langley Research Center Hampton, VA 23665. Also, research was supported in part by AFOSR Contract 85-0189.

⁺ Research supported in part by AFOSR Grant No. 86-0154.

⁺⁺ Research supported in part by NSF Grant No. DMS-8601363.

^{*} Research supported in part by DOE Grant No. DE-A505-81ER10954, NSF Grant No. MCS-821473, AFOSR Grant No. 85-0052.

1. Introduction.

The SOR method (successive overrelaxation) is a standard iterative method for solving linear systems of equations, particularly large sparse systems arising from partial differential equations. Convergence of the method is greatly affected by the choice of overrelaxation parameter ω . A standard model problem for analyzing SOR is the system of equations arising from a finite difference discretization of Laplace's equation on a rectangle with zero boundary data. The solution of this problem is identically zero; hence, the iterates of SOR also represent the error at each step. The convergence properties of SOR for the model problem also apply to Poisson's equation with general Dirichlet boundary data, since the errors will still satisfy the homogeneous equation.

Using the five-point approximation to the Laplacian gives

$$\begin{aligned} u_{j-1,k} + u_{j+1,k} + u_{j,k-1} + u_{j,k+1} - 4u_{jk} &= 0, \quad j, k = 1, 2, \dots, N-1, \\ u_{jk} &= 0, \quad j = 0, N \quad \text{or} \quad k = 0, N, \end{aligned} \quad (1.1)$$

where u_{jk} approximates the solution $u(x_j, y_k)$ with $x_j = jh$, $y_k = kh$, and $h = 1/N$. This gives a linear system of $(N-1)^2$ equations in $(N-1)^2$ unknowns. The exact form of the matrix equation, and the form that the SOR iteration takes, depends on the order in which the unknowns u_{jk} are arranged in the vector of unknowns. Two standard orderings are the natural rowwise (NR) ordering and the Red-Black (RB) ordering, in which the grid is colored in a checkerboard fashion and the Red points are ordered before the Black points (by rows within each color). For the model problem, the optimal ω and rate of convergence are the same for both of these orderings. This model problem was analyzed by Frankel[1950] and also by Young[1950] who gave a more general theory of SOR for a wide class of matrix equations in which the matrix is "consistently ordered".

Another standard model problem is obtained by using the nine-point approximation to the Laplacian:

$$\begin{aligned} 4u_{j-1,k} + 4u_{j+1,k} + 4u_{j,k-1} + 4u_{j,k+1} + u_{j-1,k-1} + u_{j-1,k+1} \\ + u_{j+1,k-1} + u_{j+1,k+1} - 20u_{jk} &= 0, \quad j, k = 1, 2, \dots, N-1, \\ u_{jk} &= 0, \quad j = 0, N \quad \text{or} \quad k = 0, N \end{aligned} \quad (1.2)$$

Again there are various ways to order the unknowns, but none of these leads to a consistently ordered matrix and so the theory of Young does not apply. Multicolor orderings, similar to the RB ordering mentioned above but usually involving four colors for the nine-point stencil, are of particular interest for parallel processing applications. Recently Adams and Jordan[1986] have studied this problem in a more general context and identified 72 distinct four color orderings. These can be grouped into equivalence classes that are known to have the same convergence behavior. For the model problem considered here, their theory reduces these to three classes of orderings that could potentially have different convergence rates, although the actual rate was not determined for any class.

In this paper, we show that in fact two of these classes are equivalent and also have the same convergence behavior as the natural rowwise ordering. The third class is shown to be distinct, with a different optimal ω and convergence rate. In each case the eigenvectors of the iteration matrix are determined. The eigenvalues (which determine the convergence rate) are found in terms of the roots of quartic equations. The optimal ω for small h is given by an asymptotic expansion about $h = 0$, and is based on an unproved assumption about which frequencies dominate the error decay. However, this approximation agrees very well with values obtained numerically for small h .

In Section 2 we use a separation of variables technique to determine the eigenvalues and eigenvectors for the NR ordering. The resulting quartic equation is used to derive the expansion for the optimal ω . Our results for this ordering differ from those given by Garabedian[1956]. We explain why both results are, in a sense, correct.

In Section 3 we discuss the various multicolor orderings. The main technique we use is a change of variables from n , the iteration number, to ν , the "data flow time", as defined by Adams and Jordan[1986]. The fact that this change of variables can be used to simplify and relate various SOR methods was observed by LeVeque and Trefethen[1986]. They present a simple Fourier analysis of SOR on the five-point stencil and show the equivalence of NR and RB using a change of variables motivated by Garabedian[1956] that is equivalent to the data flow times.

In Section 4 we analyze a pseudo-SOR method based on a Red-Black coloring for the nine-point stencil. Although this method has attractive features for parallel computers, we show that it is unsatisfactory, being an order of magnitude slower than the true SOR methods with optimal ω .

Finally, in Section 5, we briefly discuss line SOR methods and compare their convergence rates with the point SOR methods discussed in this paper.

2. Analysis of the natural rowwise ordering.

For the nine point stencil with NR ordering, the SOR method takes the form

$$\begin{aligned} u_{jk}^{n+1} = & (1-\omega) u_{jk}^n + \frac{\omega}{5} (u_{j,k-1}^{n+1} + u_{j-1,k}^{n+1} + u_{j+1,k}^n + u_{j,k+1}^n) \\ & + \frac{\omega}{20} (u_{j-1,k+1}^n + u_{j-1,k-1}^{n+1} + u_{j+1,k+1}^n + u_{j+1,k-1}^{n+1}). \end{aligned} \quad (2.1)$$

We assume that this iteration has a solution of the form

$$u_{jk}^n = \lambda^n w(x_j, y_k). \quad (2.2)$$

Then λ is an eigenvalue of the iteration matrix and the vector with components $w(x_j, y_k)$, $j, k = 1, \dots, N-1$ gives the corresponding eigenvector. Plugging (2.2) into (2.1), cancelling a common factor of λ^n , and dropping the subscripts on x and y gives

$$\begin{aligned} \lambda w(x, y) = & \lambda \omega \left[\frac{1}{5} w(x-h, y) + \frac{1}{20} w(x-h, y-h) + \frac{1}{5} w(x, y-h) + \frac{1}{20} w(x+h, y-h) \right] \\ & + \omega \left[\frac{1}{5} w(x+h, y) + \frac{1}{20} w(x-h, y+h) + \frac{1}{5} w(x, y+h) + \frac{1}{20} w(x+h, y+h) \right] \\ & + (1-\omega) w(x, y). \end{aligned} \quad (2.3)$$

The eigenfunction $w(x, y)$ must be zero on the boundary of the unit square in view of the given boundary conditions.

We use separation of variables and let $w(x, y) = X(x)Y(y)$. We also set $\alpha = \lambda^{1/2}$. Plugging this into (2.3) and dividing by $X(x)Y(y)$ gives

$$\frac{\alpha^2 + \omega - 1}{\omega} = \frac{1}{5} \left[\frac{\alpha^2 Y(y-h) + Y(y+h)}{Y(y)} \right] + \frac{1}{20} \left[\frac{\alpha^2 Y(y-h) + Y(y+h)}{Y(y)} \right] \left[\frac{X(x-h) + X(x+h)}{X(x)} \right] + \frac{1}{5} \left[\frac{\alpha^2 X(x-h) + X(x+h)}{X(x)} \right]. \quad (2.4)$$

Now let

$$Y(y) = \alpha^{y/h} \sin \eta y \quad (2.5)$$

to get

$$\frac{\alpha^2 + \omega - 1}{\omega} = \frac{2\alpha}{5} \cos \eta h + \frac{X(x-h)}{X(x)} \Phi_1 + \frac{X(x+h)}{X(x)} \Phi_2 \quad (2.6)$$

where

$$\begin{aligned} \Phi_1 &= \frac{1}{5} \alpha^2 + \frac{\alpha}{10} \cos \eta h \\ \Phi_2 &= \frac{1}{5} + \frac{\alpha}{10} \cos \eta h. \end{aligned} \quad (2.7)$$

We note that Φ_1 and Φ_2 are independent of x and y and let

$$X(x) = (\Phi_1 / \Phi_2)^{x/2h} \sin \xi x. \quad (2.8)$$

Then

$$\frac{\Phi_1 X(x-h) + \Phi_2 X(x+h)}{X(x)} = 2\Phi_1^{1/2} \Phi_2^{1/2} \cos \xi h$$

and using this in (2.6) gives

$$\frac{\alpha^2 + \omega - 1}{\omega} - \frac{2\alpha}{5} \cos \eta h = 2\Phi_1^{1/2} \Phi_2^{1/2} \cos \xi h. \quad (2.9)$$

Squaring (2.9), using (2.7), and rearranging terms gives a quartic equation for α :

$$\begin{aligned} \alpha^4 - \left[\frac{4}{5} \omega \cos \eta h + \frac{2}{25} \omega^2 \cos^2 \xi h \cos \eta h \right] \alpha^3 \\ - \left[2(1 - \omega) - \frac{4}{25} \omega^2 \cos^2 \eta h + \frac{1}{25} \omega^2 \cos^2 \xi h (\cos^2 \eta h + 4) \right] \alpha^2 \\ + \left[\frac{4}{5} \omega (1 - \omega) \cos \eta h - \frac{2}{25} \omega^2 \cos^2 \xi h \cos \eta h \right] \alpha + (1 - \omega)^2 = 0 \end{aligned} \quad (2.10)$$

An eigenmode of the iteration matrix thus has the form

$$\begin{aligned} u_{jk}^n &= \lambda^n X(x_j) Y(y_k) \\ &= \alpha^{2n+k} [(\Phi_1/\Phi_2)^{1/2}]^j \sin \xi x_j \sin \eta y_k. \end{aligned} \quad (2.11)$$

In order for the boundary conditions to be satisfied, ξ and η must be integer multiples of π . The eigenvalue is $\lambda = \alpha^2$, where α is a root of (2.10). Note that we must choose the correct square root of Φ_1/Φ_2 in (2.11) (recall that we squared (2.9) to obtain (2.10), introducing additional solutions). The correct sign for $\Phi_1^{1/2}\Phi_2^{1/2}$ is determined by the requirement that (2.9) be satisfied, and this gives the correct sign for $\Phi_1^{1/2}/\Phi_2^{1/2}$ as well.

The frequencies ξ and η each range over the values $\pi, 2\pi, \dots, (N-1)\frac{\pi}{2}$. This gives a set of $(N-1)^2/4$ pairs of frequencies. Corresponding to each pair (ξ, η) there are four roots of the quartic (2.10). In general these roots are distinct, and so we obtain $(N-1)^2$ eigenvalues and eigenvectors, the correct number. When the roots are not distinct, principal vectors will be obtained and the number of eigenvectors will be less than $(N-1)^2$. Recall that for the 5-point discretization, a principal vector was associated with the optimal ω , (see e.g. Young[1971]). We make no attempt here to determine the principal vectors or the values of ω for which they occur. However, by continuity, we do obtain all of the eigenvalues.

The frequencies $(\frac{N-1}{2}+1)\pi, \dots, (N-1)\pi$, which one might expect to be included as well, give repeats of the eigenvectors already found. Replacing ξ by $N\pi-\xi$ leaves (2.10) unchanged while replacing η by $N\pi-\eta$ simply negates the coefficients of α and α^3 . In either case the squares of the roots are unchanged. The eigenmodes (2.11) are also unchanged by these frequency reflections.

The convergence rate of the method (for fixed ω) is determined by the spectral radius of the iteration matrix, which is

$$\rho = \max_{\xi, \eta} |\lambda(\xi, \eta)|.$$

To determine the optimal ω , we need to minimize ρ over ω .

To help characterize the roots of (2.10), we first solved the quartic numerically for various values of the parameters. For example, the solid lines in Figure 2.1 (the x's will be explained later) show the magnitude of the four roots plotted as a function of ω when $\xi=\eta=\pi$ for $h=1/10$, $1/100$, and $1/1000$. When ω is small there are four real roots. As ω increases, two of the roots become complex conjugates. The optimal ω apparently occurs when these complex roots intersect the largest real root. As ω increases further, two more roots become complex conjugates and near $\omega=2$ there are two complex conjugate pairs. The same behavior was observed for smaller values of h using various values of ξ and η .

In all our experiments with various values of h , $\xi=\eta=\pi$ produced the largest root at each ω and hence the optimal ω can presumably be determined by minimizing the roots for this particular combination of frequencies. This is consistent with what is known to be true for the five-point model problem, but we have not been able to prove that this is correct for the nine-point stencil.

These observations suggest a strategy for determining the optimal ω for small h when $\xi=\eta=\pi$. We first find the roots of (2.10) when $h=0$ and then expand about these roots and equate the modulus of the roots to get the optimal ω . As $h \rightarrow 0$, the optimal ω approaches 2. Setting $h=0$ and $\omega=2$ in (2.10) gives

$$\alpha^4 - \frac{48}{25}\alpha^3 + \frac{46}{25}\alpha^2 - \frac{48}{25}\alpha + 1 = 0. \quad (2.12)$$

The roots of (2.12) are

$$\alpha_1=1, \alpha_2=1, \alpha_3=e^{i\theta}, \alpha_4=e^{-i\theta} \quad (2.13)$$

where $\theta=\cos^{-1}(-1/25)$.

First, we expand the real root at ω_{opt} about $\alpha_1=1$. We set

$$\alpha = 1 - c_1 h - c_2 h^2, \quad (2.14a)$$

$$\omega = 2 - k_1 h - k_2 h^2 \quad (2.14b)$$

and substitute into (2.10). After equating coefficients of h^2 we get

$$13c_1^2 - 15k_1c_1 + 18\pi^2 = 0, \quad (2.15)$$

which determines c_1 as a function of k_1 .

Next we expand about $e^{i\theta}$, setting

$$\alpha = e^{i\theta} (1 - \beta h) \quad (2.16)$$

and again take ω of the form (2.14b). Substituting into (2.10) and equating coefficients of h gives

$$\beta (4e^{4i\theta} - \frac{144}{25}e^{3i\theta} + \frac{92}{25}e^{2i\theta} - \frac{48}{25}e^{i\theta}) = k_1 (\frac{28}{25}e^{3i\theta} - \frac{46}{25}e^{2i\theta} + \frac{68}{25}e^{i\theta} - 2) \quad (2.17)$$

which determines β as a function of k_1 :

$$\beta = .423077 k_1. \quad (2.18)$$

Recall that $\lambda = \alpha^2$ is the eigenvalue we seek, so we equate $|\alpha^2|$ from (2.14a) and $|\alpha^2|$ from (2.16) to highest order to get

$$1 - 2c_1h + O(h^2) = 1 - 2\beta h + O(h^2),$$

and so $c_1 = \beta$. Plugging this into (2.15) and using (2.18) allows us to solve for k_1 ,

$$k_1 \approx 2.11624\pi. \quad (2.19)$$

Consequently,

$$c_1 \approx .89533\pi. \quad (2.20)$$

Using these values in (2.14a) and (2.14b), we find that the optimal ω and the corresponding spectral radii have approximate values

$$\begin{aligned} \omega_{\text{opt}} &\approx 2 - 2.11624\pi h, \\ \rho_{\text{opt}} &\approx \alpha_{\text{opt}}^2 \approx 1 - 2c_1h \approx 1 - 1.79066\pi h \end{aligned} \quad (2.21)$$

for small h .

For comparison, the corresponding values for the five-point model problem are

$$\omega_{\text{opt}}^{5\text{-pt}} \approx 2 - 2\pi h,$$

$$\rho_{\text{opt}}^{5\text{-pt}} \approx 1 - 2\pi h.$$

Notice that for the nine-point stencil, the spectral radius is slightly larger, giving somewhat slower convergence than for the five-point stencil, although the two are very close. Most importantly, both are $1 - O(h)$ as $h \rightarrow 0$, giving asymptotically the same order of convergence. By contrast the Jacobi and Gauss-Seidel methods, and also the pseudo-SOR method analyzed in Section 4, have spectral radius $1 - O(h^2)$ as $h \rightarrow 0$.

It is very interesting to compare these results with asymptotic results obtained by Garabedian[1956], especially since they do not agree and yet both are, in a sense, correct. Garabedian's analysis is based on viewing the SOR iteration (2.1) as a finite difference method for a time-dependent PDE. Expanding in Taylor series shows that this difference equation is consistent with the PDE

$$\begin{aligned} 5Cu_t + 2u_{xt} + 3u_{yt} &= 3u_{xx} + 3u_{yy} \\ u &= 0 \text{ on the boundary} \end{aligned} \quad (2.22)$$

where C and ω are related by

$$\omega = \frac{2}{1+Ch}. \quad (2.23)$$

If we fix $C > 0$ and choose ω according to (2.23) for each $h > 0$ then $0 < \omega < 2$ and so the method (2.1) is stable. Since it is consistent with the linear equation (2.22), iterates u_{jk}^n with $n=T/h$ must converge to solutions $u(x_j, y_k, T)$ of the PDE (2.22) as $h \rightarrow 0$ (by the Lax Equivalence Theorem) if we choose u_{jk}^0 by discretizing fixed initial data $u(x, y, 0)$. Consequently, studying the decay of solutions to (2.22) gives information about the rate of convergence of SOR.

By introducing the change of variables

$$s = t + \frac{x}{3} + \frac{y}{2} \quad (2.24)$$

(2.22) is transformed to

$$5Cu_s + \frac{13}{12}u_{ss} = 3u_{xx} + 3u_{yy}. \quad (2.25)$$

Separation of variables shows that eigenmodes of this PDE have the form

$$u(x, y, s) = e^{-ps} \sin \xi x \sin \eta y \quad (2.26)$$

where ξ and η are integer multiples of π and $p=p(\xi, \eta)$ is a root of the quadratic equation

$$\frac{13}{12}p^2 - 5Cp + 3(\xi^2 + \eta^2) = 0. \quad (2.27)$$

Transforming back to the original time variable gives

$$u(x, y, t) = e^{-p(t+x/3+y/2)} \sin \xi x \sin \eta y. \quad (2.28)$$

Note that in a time step of length h , this solution decays by a factor $e^{-\text{Re}(p)h}$. The eigenmode with slowest decay is obtained by taking $\xi=\eta=\pi$ and the negative square root in solving (2.27) giving

$$p_{\min} = \frac{6}{13} \left[5C - \sqrt{25C^2 - 26\pi^2} \right] \quad (2.29)$$

If we obtain initial data for SOR by discretizing the corresponding eigenfunction, $u_{jk}^0 = u(x_j, y_k, 0)$ from (2.28), it follows (by convergence) that the decay factor for the SOR iteration must have the form

$$\lambda_{\max} = 1 - \text{Re}(p_{\min})h + O(h^2) \quad (2.30)$$

as $h \rightarrow 0$. Since taking other eigenfunctions as initial data gives faster decay, one is led to the conclusion that in order to obtain the fastest possible convergence, we should maximize $\text{Re}(p_{\min})$ and hence minimize λ_{\max} . Recall that the value of C is still at our disposal. We can minimize $\text{Re}(p_{\min})$ by setting the radical to zero in (2.29), giving

$$C = \frac{\sqrt{26}}{5}\pi \approx 1.02\pi, \quad p_{\min} = 6\pi\sqrt{2/13} \approx 2.35\pi. \quad (2.31)$$

By (2.23) and (2.30) we obtain the following predictions for the optimal ω and the corresponding decay rate, as in Garabedian[1956]:

$$\begin{aligned} \omega_{\text{opt}}^* &= \frac{2}{1+Ch} \approx 2(1-Ch) = 2 - 2.04\pi h \\ \rho_{\text{opt}}^* &= e^{-p_{\min}h} \approx 1 - p_{\min}h = 1 - 2.35\pi h. \end{aligned} \quad (2.32)$$

These values do not agree with the values (2.21) found by computing the eigenvalues of the iteration matrix. The reason is the following. While (2.30) does indeed give a correct expression for the largest eigenvalue of the iteration matrix corresponding to a decay factor for the PDE, there are other, spurious, eigenvalues of the discrete problem that have larger magnitude for ω near 2 and hence determine the spectral radius ρ . This is seen clearly in Figure 2.1 where we have plotted $|e^{-p_h}|$ for the two roots of the quadratic (2.27) (as +'s) along with $|\lambda|$, the magnitudes of the actual eigenvalues obtained by solving the quartic (2.10) (as the solid lines). One pair of discrete eigenvalues closely matches $|e^{-p_h}|$ for small h while the other (complex conjugate) pair does not. In fact, Garabedian's results may also be obtained from our approach by choosing k_1 in (2.15) to maximize c_1 , thereby ignoring the effect of the other root.

For each fixed h , we can choose initial data (namely, as a spurious eigenvector) so that convergence is slow and determined by the spectral radius. On the other hand, these spurious eigenvectors become highly oscillatory and are not convergent as $h \rightarrow 0$. Consequently, if we obtain our initial data by discretizing a fixed function of x and y at each h (as is more realistic in practice), we would expect to see vanishingly small components of these spurious eigenvectors as $h \rightarrow 0$. For practical purposes, then, the values (2.32) obtained by Garabedian may be more meaningful and useful than the "true" values (2.21).

This is demonstrated in Figure 2.2 where we show the decay of $\|u\|_2$ for various initial data. For initial data obtained by discretizing the smooth data $u(x,y) = (x^2 - x)(y^2 - y)$, the observed decay is much closer to λ_{\max}^n , as predicted by (2.30), than to ρ^n .

To verify that the eigenvector corresponding to the spectral radius is highly oscillatory, we note that by (2.5) and (2.8) an eigenvector has the form

$$w_{jk} = \alpha^k [(\Phi_1/\Phi_2)^{1/2}]^j \sin \xi x_j \sin \eta y_k. \quad (2.33)$$

At the point ω_{opt} , the maximum eigenvalue corresponds to a value of α given by (2.16). Inserting this in (2.33) gives

$$w_{jk} = e^{i\theta k} (1 - \beta h)^k [(\Phi_1/\Phi_2)^{1/2}]^j \sin \xi x_j \sin \eta y_k. \quad (2.34)$$

Since $\theta = \cos^{-1}(-1/25)$, this function will be oscillatory in k and nonconvergent as $h \rightarrow 0$.

By contrast, the eigenvector corresponding to the other pair of roots converges to the eigenfunctions (2.28) of the PDE as $h \rightarrow 0$. For these vectors our previous arguments show that λ has the form of (2.30) and hence α , the square root of λ , can be expressed as

$$\alpha = 1 - \frac{1}{2}ph + O(h^2). \quad (2.35)$$

Expanding Φ_1/Φ_2 using this value of α in (2.7) shows that

$$\Phi_1/\Phi_2 = 1 - \frac{2}{3}ph + O(h^2). \quad (2.36)$$

Plugging (2.35) and (2.36) into (2.11) gives

$$\begin{aligned} u_{jk}^n &= (1 - \frac{1}{2}ph + O(h^2))^{2n+k} (1 - \frac{1}{3}ph + O(h^2))^j \sin \xi_j h \sin \eta_k h \\ &= (1 - ph + O(h^2))^{n+j/3+k/2} \sin \xi_j h \sin \eta_k h. \end{aligned} \quad (2.37)$$

As $h \rightarrow 0$ with $t = nh$, $x = jh$ and $y = kh$ fixed, this approaches the eigenmode (2.28) of the PDE.

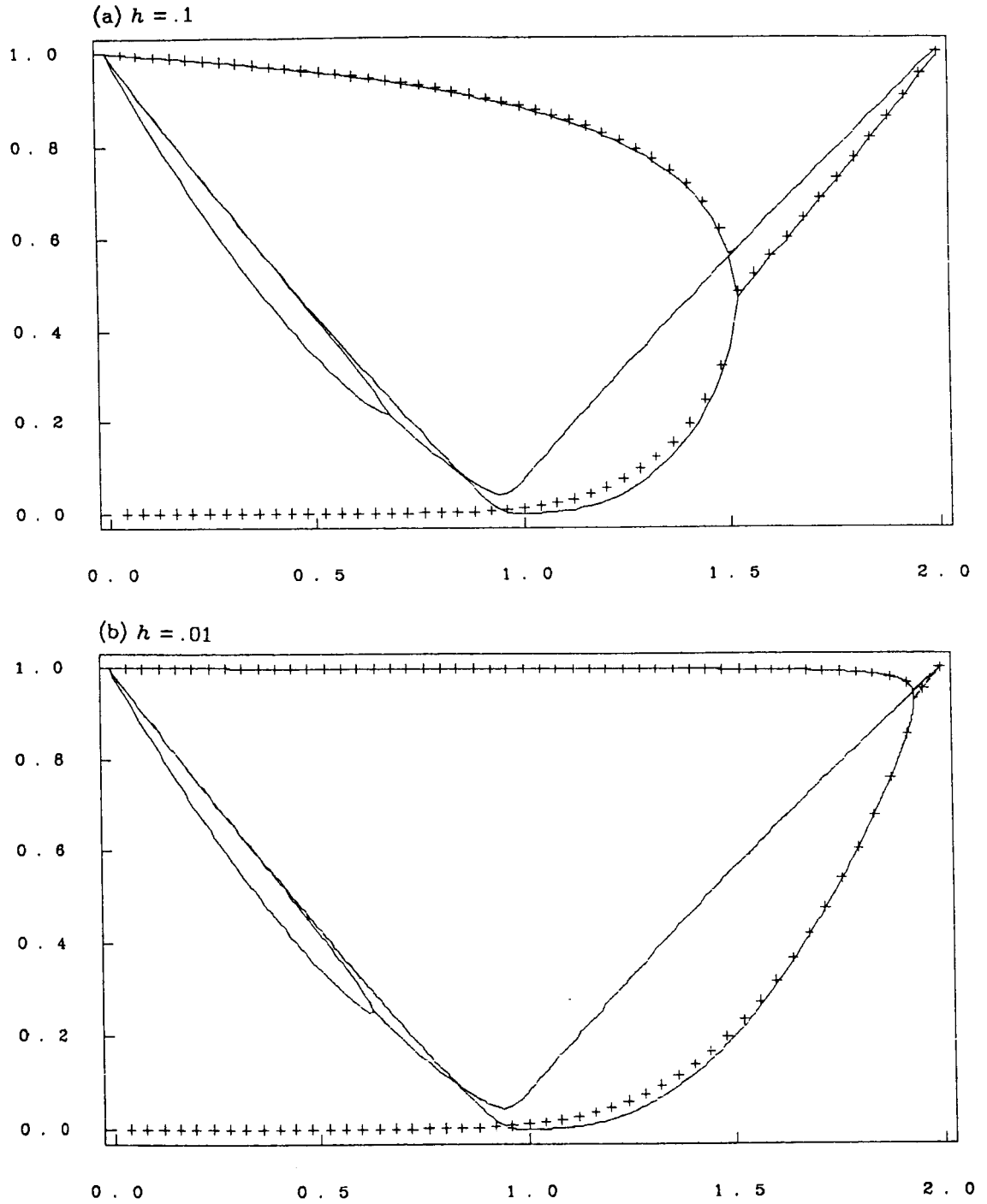
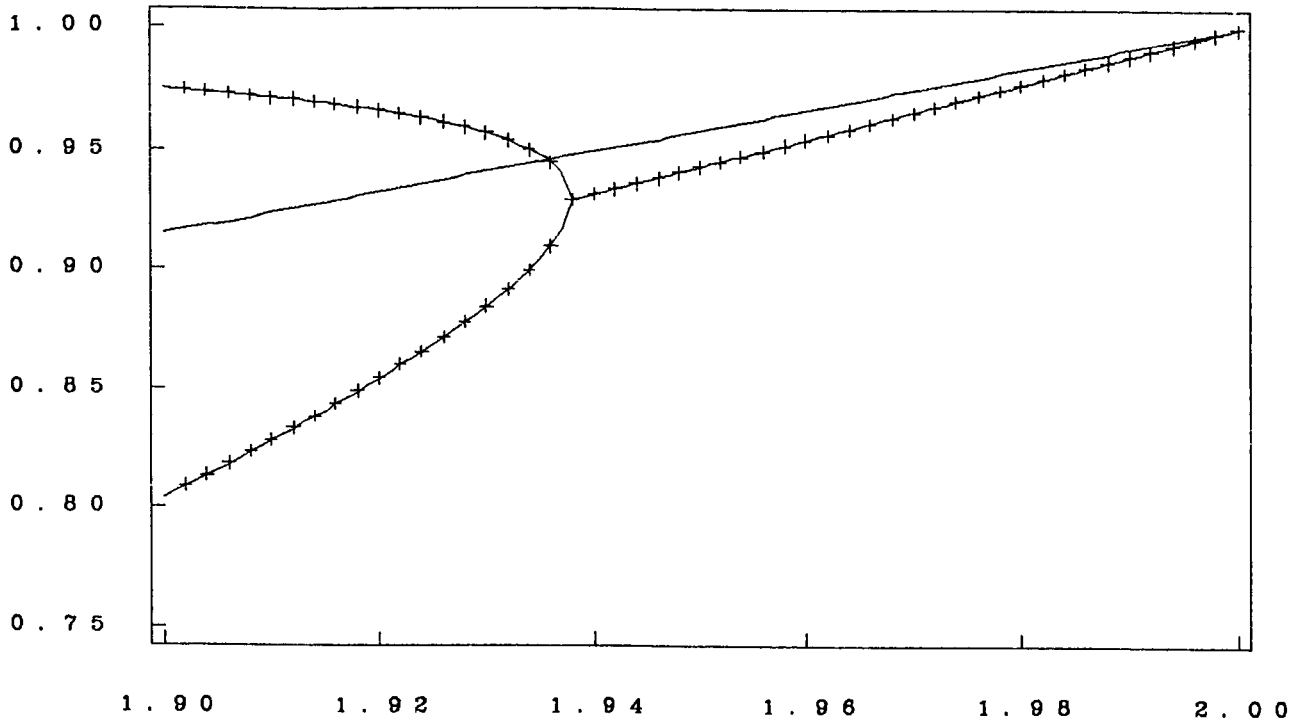
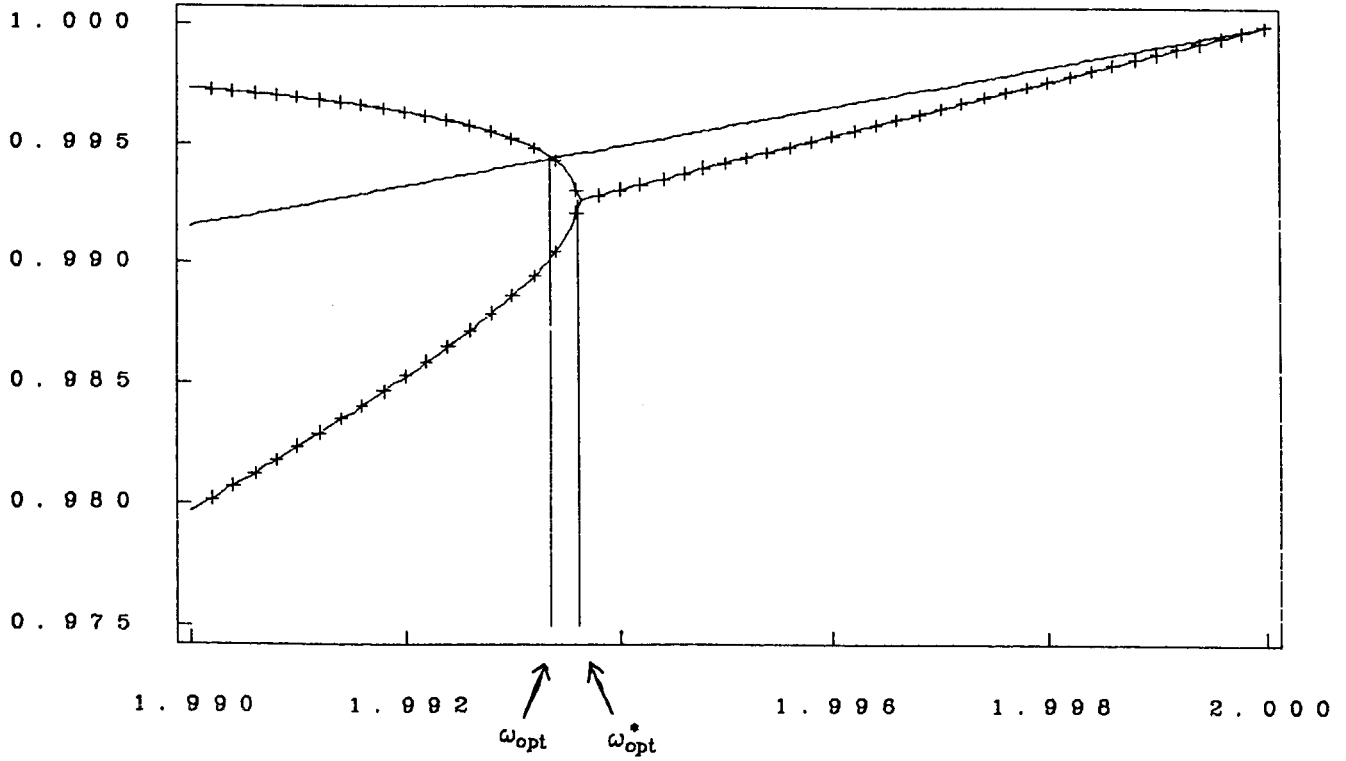


Figure 2.1. Solid lines show $|\alpha^2| = |\lambda|$ for the iteration matrix with $\xi = \eta = \pi$, obtained by solving the quartic (2.10). The symbols + show e^{-ph} where p is a root of the quadratic equation (2.27) with $\xi = \eta = \pi$.

- (a) $h = .1$ for $0 \leq \omega \leq 2$.
- (b) $h = .01$ for $0 \leq \omega \leq 2$.
- (c) $h = .01$ for $1.9 \leq \omega \leq 2$.
- (d) $h = .001$ for $1.99 \leq \omega \leq 2$.

(c) $h = .01$ (d) $h = .001$ 

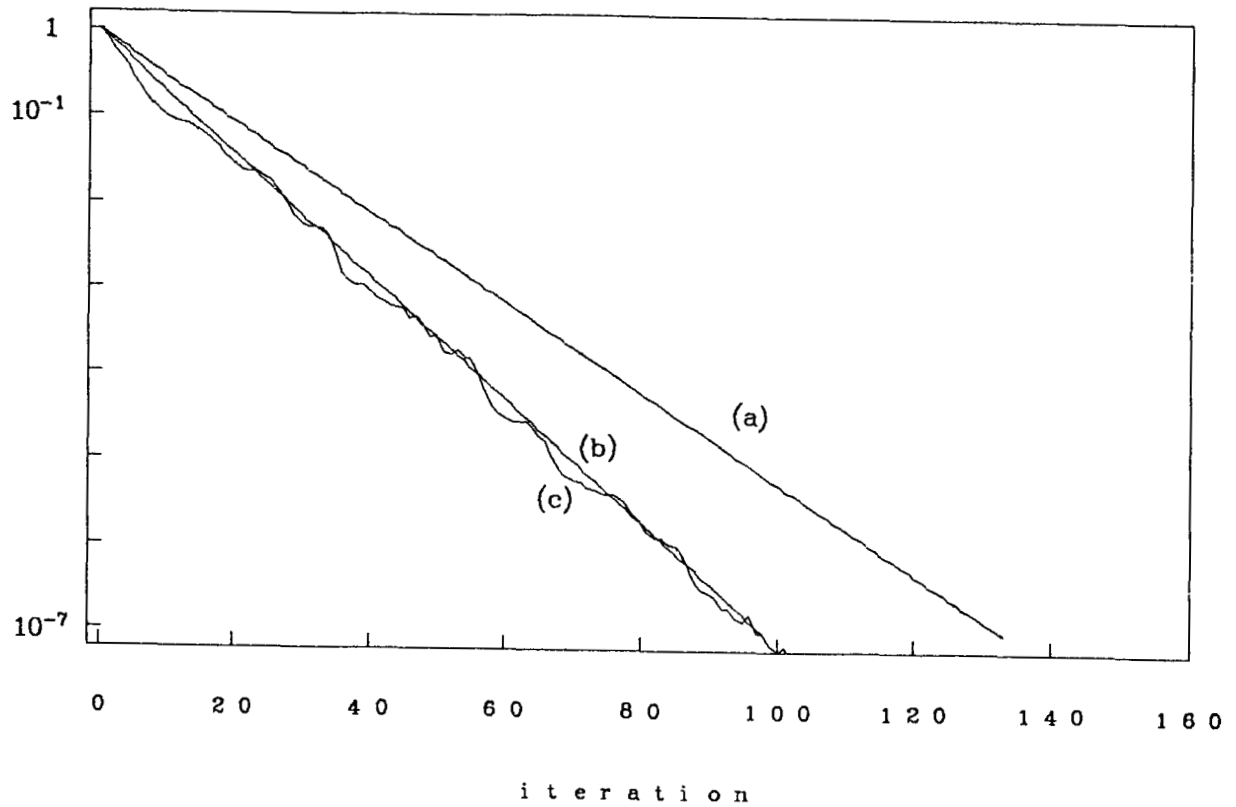


Figure 2.2. Convergence history (2-norm of error versus iteration number) for the NR ordering with $h = 0.05$ and $\omega = 1.86$. Three choices of initial data are compared:

- (a) An eigenvector corresponding to the spectral radius.
- (b) An eigenvector corresponding to the largest nonspurious eigenvalue.
- (c) $u_{jk}^0 = (x_j^2 - x_j)(y_k^2 - y_k)$.

Note that the realistic initial data (c) more closely matches (b) than (a).

3. Multicolor SOR.

In this section we consider the SOR method applied to the nine-point model problem with several alternative orderings of the unknowns u_{jk} . These orderings are determined by labeling the grid points with four different colors (Red, Black, Green and Orange) and then ordering the points by first listing all the points of one color, then a second color, and so on. The overall ordering of grid points is determined by two factors: a) the manner in which the grid points are labeled (the coloring of the grid) and b) the order in which the colors are taken (the ordering of the colors).

Four-colorings are of interest for the nine-point stencil because with four colors it is possible to decouple the grid, in the sense that the resulting SOR formula for updating a grid point of any given color involves neighboring grid points, all of which have different colors than the center point. This is advantageous in parallel processing applications since all grid points of the same color can be updated simultaneously.

For the five-point stencil, two colors suffice to decouple the grid using the RB checkerboard pattern discussed in Section 1. Recently LeVeque and Trefethen[1986] have shown an easy way to analyze the five-point model problem using a change of variables from the iteration number, n , to the earliest time, v , that the unknown at a grid point can be updated assuming one update requires one time unit. This variable v corresponds to the "data flow times" discussed in Adams and Jordan[1986] and closely resembles the change of variables used by Garabedian[1956] to analyze the PDE. This change of variables allows the use of Fourier analysis to determine the convergence rate and optimal ω . It also gives a straightforward proof of the equivalence of the NR and RB orderings.

Here we use this same approach to analyze the four-color orderings for the nine-point stencil. Before introducing these orderings, we briefly review the analysis for the five-point NR and RB orderings to introduce notation and motivate our nine-point analysis.

For the five-point model problem (1.1) with the NR ordering, the SOR iteration takes the form

$$u_{jk}^{n+1} = (1-\omega) u_{jk}^n + \frac{\omega}{4} (u_{j-1,k}^{n+1} + u_{j,k-1}^{n+1} + u_{j,k+1}^n + u_{j+1,k}^n). \quad (3.1)$$

The stencil for updating a grid point on iteration $n+1$ using the NR ordering is given in Figure 3.1

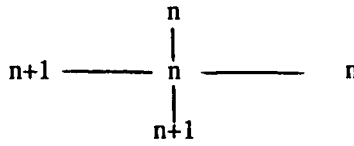


Figure 3.1. NR Stencil in Variable n

To assist in determining the change of variables, the earliest times at which an unknown can be updated on the first two iterations using the stencil in Figure 3.1 are listed below each node in Figure 3.2.

4,6	5,7	6,8	7,9
3,5	4,6	5,7	6,8
2,4	3,5	4,6	5,7
1,3	2,4	3,5	4,6

Figure 3.2. Times for 2 Iterations of NR

These times define the iteration variable v . Each node in Figure 3.2 is updated at time $v+1$ by the stencil shown in Figure 3.3,

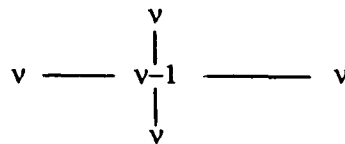


Figure 3.3. NR Stencil in Variable v

and the corresponding SOR iteration is

$$u_{jk}^{v+1} = (1-\omega) u_{jk}^{v-1} + \frac{\omega}{4} (u_{j-1,k}^v + u_{j,k-1}^v + u_{j,k+1}^v + u_{j+1,k}^v). \quad (3.2)$$

Figure 3.2 shows that the times along lines $j+k$ are constant and that iterations in variable n occur every 2 time units. Hence, the proper change of variables between (3.1) and (3.2) is

$$v = 2n + j + k - 2. \quad (3.3)$$

The advantage of this change of variables is that the eigenmodes of (3.2) are easy to determine - they are simply Fourier modes of the form

$$u_{jk}^v = g^v \sin \xi x_j \sin \eta y_k. \quad (3.4)$$

These grid functions satisfy the boundary conditions provided that ξ and η are integer multiples of π , and substituting into (3.2) gives the following equation for g :

$$g^2 = (1-\omega) + \frac{\omega g}{2} (\cos \xi h + \cos \eta h). \quad (3.5)$$

For each ξ and η , this equation has two solutions, giving two eigenmodes. We obtain all modes by letting ξ and η range over the values $\xi, \eta = \pi, 2\pi, \dots, (N-1)\pi$, for a total of $2(N-1)^2$ modes. This is correct since (3.2) requires two previous levels of data to calculate u_{jk}^{v+1} .

By the change of variables (3.3), an eigenvalue λ of (3.1) is seen to be g^2 and the corresponding eigenvector has components $g^{j+k} \sin \xi x_j \sin \eta y_k$. We now appear to have twice as many eigenmodes as required for (3.1), but here each mode is repeated since replacing (ξ, η) by $(N\pi - \xi, N\pi - \eta)$ simply negates the roots of (3.5). Since $\lambda = g^2$ this reflection leaves these eigenvalues unchanged. The eigenvector is also unchanged since

$$(-g)^{j+k} \sin(N\pi - \xi)x_j \sin(N\pi - \eta)y_k = g^{j+k} \sin \xi x_j \sin \eta y_k.$$

Equation (3.5) gives the famous relationship between an eigenvalue λ of SOR and an eigenvalue $\mu = \frac{1}{2} (\cos \xi h + \cos \eta h)$ of Jacobi:

$$\frac{\lambda + \omega - 1}{\omega} = \lambda^{1/2} \mu. \quad (3.6)$$

Equation (3.6) can be used to determine the optimal value of ω as a function of μ (see e.g. Young[1971]) and will not be repeated here.

A similar analysis can be done for the Red/Black ordering of the grid points. In the variable n there are two stencils, one for the Red nodes and one for the Black ones, as given in Figure 3.4.

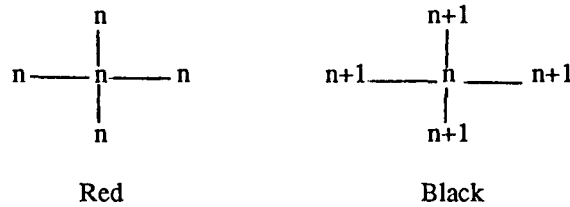


Figure 3.4. Red/Black Stencil in Variable n

The corresponding iteration is

$$\begin{aligned} R: u_{jk}^{n+1} &= (1-\omega) u_{jk}^n + \frac{\omega}{4} (u_{j,k+1}^n + u_{j,k-1}^n + u_{j-1,k}^n + u_{j+1,k}^n) \\ B: u_{jk}^{n+1} &= (1-\omega) u_{jk}^n + \frac{\omega}{4} (u_{j,k+1}^{n+1} + u_{j,k-1}^{n+1} + u_{j-1,k}^{n+1} + u_{j+1,k}^{n+1}). \end{aligned} \quad (3.7)$$

The earliest times corresponding to Figure 3.4 are given in Figure 3.5.

B	R	B	R
2,4	1,3	2,4	1,3
R	B	R	B
1,3	2,4	1,3	2,4
B	R	B	R
2,4	1,3	2,4	1,3
R	B	R	B
1,3	2,4	1,3	2,4

Figure 3.5. Times for 2 Iterations of RB

In the data flow variable, v , both R and B nodes have the same stencil; namely, the stencil of Figure 3.3. Equation (3.2) gives the update formula for all nodes. Hence, (3.5) and (3.6) also hold for the R/B ordering. Figure 3.5 shows that the times along all lines with $j+k$ even are equal and similarly for $j+k$ odd and iterations in variable n occur every 2 time units in v . Therefore, the change of variables is

$$v = 2n + (j+k) \bmod 2 - 1 \quad (3.8)$$

and the eigenvector components of this iteration corresponding to ξ, η are

$$w_{jk} = \begin{cases} \sin \xi x_j \sin \eta y_k \\ \lambda^{1/2} \sin \xi x_j \sin \eta y_k \end{cases}$$

for the R and B nodes respectively. This agrees with that given in Young[1950].

We now turn to the nine-point stencil, with orderings based on four colors. The results of Adams and Jordan[1986] applied to this model problem show that the 72 distinct four color orderings can be grouped into three equivalence classes with regard to convergence behavior:

- Ordering #1: The grid is colored as in Figure 3.6a with ordering R/B/G/O.
 Ordering #2: The grid is colored as in Figure 3.6b with ordering R/B/G/O.
 Ordering #3: The grid is colored as in Figure 3.6b with ordering R/B/O/G.

G O R B	G O G O
R B G O	R B R B
G O R B	G O G O
R B G O	R B R B

Figure 3.6a.

Figure 3.6b.

We will show that Orderings #1 and #2 are in fact equivalent, both being equivalent to the NR ordering discussed in Section 2. Ordering #3 is different however, and gives slightly slower convergence based on the spectral radius and slightly faster convergence based on the eigenvalue that dominates the iteration in practice.

Ordering #1: Figure 3.7 shows the update times for this ordering which define the data flow variable v .

G	O	R	B
3,7	4,8	1,5	2,6
R	B	G	O
1,5	2,6	3,7	4,8
G	O	R	B
3,7	4,8	1,5	2,6
R	B	G	O
1,5	2,6	3,7	4,8

Figure 3.7. Times for two iterations with Ordering #1

In this variable, each node has the same stencil with update formula

$$u_{jk}^{v+4} = (1 - \omega)u_{jk}^v + \frac{\omega}{5} (u_{j-1,k}^{v+3} + u_{j+1,k}^{v+1} + u_{j,k+1}^{v+2} + u_{j,k-1}^{v+2}) + \frac{\omega}{20} (u_{j-1,k-1}^{v+1} + u_{j-1,k+1}^{v+1} + u_{j+1,k-1}^{v+3} + u_{j+1,k+1}^{v+3}). \quad (3.9)$$

The change of variables is given by

$$v = 4n + c - 3 \quad (3.10)$$

where $c = 0, 1, 2, 3$ for the R, B, G, and O nodes of Figure 3.7, respectively.

To see that this ordering is equivalent to the NR ordering, we only need to look at the update times for the NR ordering, shown in Figure 3.8.

7,11	8,12	9,13	10,14
5,9	6,10	7,11	8,12
3,7	4,8	5,9	6,10
1,5	2,6	3,7	4,8

Figure 3.8. Times for the 9 point NR Ordering

If we define the variable v by these times, we again obtain iteration (3.9) with the change of variables

$$v = 4n + 2k + j - 6. \quad (3.11)$$

Since a change of variables gives (3.9) in either case, the eigenvalues and hence convergence behavior will be identical. If g is an eigenvalue of (3.9) then $\lambda = g^4$ is an eigenvalue of both NR and Ordering #1.

The eigenvectors, however, will not be the same since a different change of variables is used in each case. The eigenvectors for the NR ordering were determined in Section 2. Using these and the above changes of variables allows us to determine the eigenvectors for Ordering #1. In analyzing (3.9) we view it as applying to all mesh points (j,k) at each level of v , although in our applications it is applied only to points of a single color in each step. (Note that we could apply it to all points without affecting the results, but that the work required would be increased by a factor of 4.) Since (3.9) requires four levels of prior data to determine u_{jk}^{v+4} , an eigenvector of (3.9) consists of $4(N-1)^2$ values,

$$V = \begin{bmatrix} V^0 \\ V^1 \\ V^2 \\ V^3 \end{bmatrix}$$

where $V^v = \{V_{jk}^v\}$ for $j, k = 1, 2, \dots, N-1$. If g is the corresponding eigenvalue, then

$$\begin{bmatrix} V^1 \\ V^2 \\ V^3 \\ V^4 \end{bmatrix} = g \begin{bmatrix} V^0 \\ V^1 \\ V^2 \\ V^3 \end{bmatrix}.$$

This indicates that $V^{v+1} = gV^v$ for each v and hence

$$V = \begin{bmatrix} V^0 \\ gV^0 \\ g^2V^0 \\ g^3V^0 \end{bmatrix} \in R^{4(N-1)^2}.$$

If we now let V_R^0 be the vector consisting only of the values V_{jk}^0 for which (j,k) is a red point, and similarly for V_B^0 , V_G^0 and V_O^0 , then an eigenvector of the original iteration in the n variable (with Ordering #1) has the form

$$V^{(\#1)} = \begin{bmatrix} V_R^0 \\ gV_B^0 \\ g^2V_G^0 \\ g^3V_O^0 \end{bmatrix} \in R^{(N-1)^2} \quad (3.12)$$

with eigenvalue $\lambda = g^4$.

On the other hand, by the change of variables (3.11), an eigenvector for the NR ordering in the n variable has the form

$$V_{jk}^{(NR)} = g^{2k+j} V_{jk}^0$$

again with eigenvalue $\lambda = g^4$. Equation (2.11) gives the eigenvector for the NR ordering,

$$V_{jk}^{(NR)} = \alpha^k [(\Phi_1/\Phi_2)^{1/2}]^j \sin \xi x_j \sin \eta y_k$$

where Φ_1 and Φ_2 are given by (2.7) and $\alpha = \lambda^{1/2} = g^2$. Using this we obtain

$$\begin{aligned} V_{jk}^0 &= g^{-2k-j} V_{jk}^{(NR)} \\ &= g^{-j} [(\Phi_1/\Phi_2)^{1/2}]^j \sin \xi x_j \sin \eta y_k. \end{aligned}$$

The eigenvectors are now determined by (3.12) with $\xi, \eta = \pi, 2\pi, \dots, (N-1)\frac{\pi}{2}$. As before, the frequencies $\xi, \eta = (\frac{N-1}{2}+1)\pi, \dots, (N-1)\pi$ give repeats of the eigenvalue-eigenvector pairs already found.

Ordering #2: For Ordering #2, the associated earliest times for the first two iterations are given in Figure 3.9.

G	O	G	O
3,7	4,8	3,7	4,8
R	B	R	B
1,5	2,6	1,5	2,6
G	O	G	O
3,7	4,8	3,7	4,8
R	B	R	B
1,5	2,6	1,5	2,6

Figure 3.9. R/B/G/O Times for Ordering #2

A quick inspection of Figure 3.9 shows that the R and G nodes have the same stencil in the variable v with the following update formula:

$$\begin{aligned}
 R, G: u_{jk}^{v+4} = & (1-\omega) u_{jk}^v + \frac{\omega}{5} (u_{j-1,k}^{v+1} + u_{j+1,k}^{v+1} + u_{j,k-1}^{v+2} + u_{j,k+1}^{v+2}) \\
 & + \frac{\omega}{20} (u_{j-1,k-1}^{v+3} + u_{j-1,k+1}^{v+3} + u_{j+1,k-1}^{v+3} + u_{j+1,k+1}^{v+3}).
 \end{aligned} \tag{3.13}$$

Likewise, the B and O nodes have the same stencil with update formula:

$$\begin{aligned}
 B, O: u_{jk}^{v+4} = & (1-\omega) u_{jk}^v + \frac{\omega}{5} (u_{j-1,k}^{v+3} + u_{j+1,k}^{v+3} + u_{j,k-1}^{v+2} + u_{j,k+1}^{v+2}) \\
 & + \frac{\omega}{20} (u_{j-1,k-1}^{v+1} + u_{j-1,k+1}^{v+1} + u_{j+1,k-1}^{v+1} + u_{j+1,k+1}^{v+1}).
 \end{aligned} \tag{3.14}$$

The change of variables from n to v is again given by (3.10), where $c = 0, 1, 2,$ and 3 for the R, B, G, and O equations respectively.

Now, the equations in (3.13) and (3.14) have the symmetry needed to verify that $V_{jk}^0 = \sin \xi x_j \sin \eta y_k$. Thus the methods in (3.13) and (3.14) have the same value for V_{jk}^0 but different amplification factors, say g_1 and g_2 . A single step of the full method, in variable n , consists of four sweeps, two with (3.13) and two with (3.14) and hence has amplification factor

$$\lambda = g_1^2 g_2^2. \tag{3.15}$$

In order to determine λ , we find $\alpha = g_1 g_2$ by considering two sweeps of the method, Red and Black, say. We substitute the following values,

$$\begin{aligned}
u_{jk}^{v+1} &= g_2 u_{jk}^v, \\
u_{jk}^{v+2} &= g_1 g_2 u_{jk}^v, \\
u_{jk}^{v+3} &= g_1 g_2^2 u_{jk}^v, \\
u_{jk}^{v+4} &= g_1^2 g_2^2 u_{jk}^v, \\
u_{jk}^{v+5} &= g_1^2 g_2^3 u_{jk}^v,
\end{aligned} \tag{3.16}$$

with

$$u_{jk}^n = e^{i(\xi x_j + \eta y_k)}$$

into (3.13) to get

$$g_1^2 g_2^2 = (1 - \omega) + \frac{\omega}{5} (2g_2 \cos \xi h + 2g_1 g_2 \cos \eta h + g_1 g_2^2 \cos \xi h \cos \eta h). \tag{3.17}$$

Next, we take a step with (3.14) to update the Black nodes, and obtain u_{jk}^{v+5} . Plugging (3.16) into (3.14) for $v+5$ we get

$$g_1^2 g_2^2 = (1 - \omega) + \frac{\omega}{5} (2g_1^2 g_2 \cos \xi h + 2g_1 g_2 \cos \eta h + g_1 \cos \xi h \cos \eta h). \tag{3.18}$$

Equations (3.17) and (3.18) can be equated and g_1 and g_2 eliminated to give a quartic equation for α . Surprisingly, this quartic is again (2.10), the quartic obtained in our analysis of the NR ordering by separation of variables. This shows that this ordering is equivalent to the NR ordering, and hence is also equivalent to Ordering #1.

The eigenvectors in variable n can be seen from (3.10) and (3.16) to be

$$V^{(n)} = \begin{bmatrix} V_R^0 \\ g_2 V_B^0 \\ g_1 g_2 V_G^0 \\ g_1 g_2^2 V_O^0 \end{bmatrix} \in R^{(N-1)^2} \tag{3.19}$$

where $V_{jk}^0 = \sin \xi x_j \sin \eta y_k$, $\xi, \eta = \pi, 2\pi, \dots, (N-1)\frac{\pi}{2}$ with eigenvalue $\lambda = g_1^2 g_2^2$. Again, we find that

eigenvalue-eigenvector pairs are repeated for the frequencies $(\frac{N-1}{2} + 1)\pi, \dots, (N-1)\pi$.

Ordering #3: For this ordering, the earliest times for the first two iterations are given in Figure 3.10.

G	O	G	O
4,8	3,7	4,8	3,7
R	B	R	B
1,5	2,6	1,5	2,6
G	O	G	O
4,8	3,7	4,8	3,7
R	B	R	B
1,5	2,6	1,5	2,6

Figure 3.10. R/B/O/G Times for Coloring #1

The R and O nodes have the same stencil in the variable v with the following update formula:

$$\begin{aligned}
 R, O: u_{jk}^{v+4} = & (1-\omega) u_{jk}^v + \frac{\omega}{5} (u_{j,k+1}^{v+3} + u_{j,k-1}^{v+3} + u_{j+1,k}^{v+1} + u_{j-1,k}^{v+1}) \\
 & + \frac{\omega}{20} (u_{j-1,k-1}^{v+2} + u_{j-1,k+1}^{v+2} + u_{j+1,k-1}^{v+2} + u_{j+1,k+1}^{v+2})
 \end{aligned} \tag{3.20}$$

Likewise, the B and G nodes are updated by the formula:

$$\begin{aligned}
 B, G: u_{jk}^{v+4} = & (1-\omega) u_{jk}^v + \frac{\omega}{5} (u_{j,k+1}^{v+1} + u_{j,k-1}^{v+1} + u_{j+1,k}^{v+3} + u_{j-1,k}^{v+3}) \\
 & + \frac{\omega}{20} (u_{j-1,k-1}^{v+2} + u_{j-1,k+1}^{v+2} + u_{j+1,k-1}^{v+2} + u_{j+1,k+1}^{v+2})
 \end{aligned} \tag{3.21}$$

Now, substituting (3.16) into (3.20) and (3.21) yields

$$g_1^2 g_2^2 = (1-\omega) + \frac{2\omega}{5} (g_1 g_2^2 \cos \eta h + g_2 \cos \xi h) + \frac{\omega}{5} g_1 g_2 \cos \eta h \cos \xi h \tag{3.22}$$

and

$$g_1^2 g_2^2 = (1-\omega) + \frac{2\omega}{5} (g_1 \cos \eta h + g_1^2 g_2 \cos \xi h) + \frac{\omega}{5} g_1 g_2 \cos \xi h \cos \eta h . \tag{3.23}$$

respectively. As before, we equate (3.22) and (3.23), eliminate g_1 and g_2 and get the following quartic in $\alpha = g_1 g_2$:

$$\begin{aligned}
& \alpha^4 - \left(\frac{2}{5} \omega \cos \eta h \cos \xi h + \frac{4}{25} \omega^2 \cos \eta h \cos \xi h\right) \alpha^3 \\
& + \left(\frac{1}{25} \omega^2 \cos^2 \eta h \cos^2 \xi h + 2(\omega-1) - \frac{4}{25} \omega^2 \cos^2 \eta h - \frac{4}{25} \omega^2 \cos^2 \xi h\right) \alpha^2 \\
& + \left(\frac{2}{5} \omega(1-\omega) \cos \eta h \cos \xi h - \frac{4}{25} \omega^2 \cos \xi h \cos \eta h\right) \alpha + (\omega-1)^2 = 0.
\end{aligned} \tag{3.24}$$

The change of variables from n to v is again given by (3.10) where $c=0, 1, 2$, and 3 corresponding to the R, B, O, and G equations, respectively. Following the same arguments as before, we find that the eigenvectors in variable n for Ordering #3 are given by

$$V^{(\#3)} = \begin{bmatrix} V_R^0 \\ g_2 V_B^0 \\ g_1 g_2 V_G^0 \\ g_1 g_2 V_O^0 \end{bmatrix} \in R^{(N-1)^2}$$

where $V_{jk}^0 = \sin \xi x_j \sin \eta y_k$, $\xi, \eta = \pi, 2\pi, \dots, (N-1)\frac{\pi}{2}$ and eigenvalue $\lambda = g_1^2 g_2^2$. Again, we find that eigenvalue-eigenvector pairs are repeated for $\xi, \eta = (\frac{N-1}{2} + 1)\pi, \dots, (N-1)\pi$. This can be seen for the eigenvalues from (3.24) since replacing (ξ, η) by $(N\pi - \xi, N\pi - \eta)$ leaves the quartic unchanged and replacing (ξ, η) by either $(N\pi - \xi, \eta)$ or $(\xi, N\pi - \eta)$ negates the coefficient of the α and α^3 terms.

The quartic in (3.24) does not agree with the quartic in (2.10) and the roots do not agree in general. Consequently the optimal ω and corresponding convergence rate are different for this ordering than for the other orderings considered so far.

Numerical results show that the roots of (3.24) have the same qualitative behavior as shown in Figure 2.1 with $\xi = \eta = \pi$ giving the slowest decay. The optimal ω again appears to occur where the two complex roots and the largest real root intersect. When $h = 0$ and $\omega = 2$, the roots satisfy

$$\alpha^4 - \frac{36}{25} \alpha^3 + \frac{22}{25} \alpha^2 - \frac{36}{25} \alpha + 1 = 0, \tag{3.25}$$

and are given by (2.13) where $\theta = \cos^{-1}(-7/25)$. The asymptotic analysis could be performed as before by expanding about the roots of (3.25), but this has not been carried out. Instead we are content to find ω_{opt} by numerically solving (3.24) and optimizing the result. This leads to

$$\begin{aligned}\omega_{\text{opt}} &\approx 2 - 2.14\pi h, \\ \rho_{\text{opt}} &\approx 1 - 1.60\pi h\end{aligned}\tag{3.26}$$

for small h . This R/B/O/G SOR iteration was programmed and the results of (3.26) confirmed. By comparing (2.21) and (3.26), we see that different evaluation orderings for the same coloring of the grid points can lead to different convergence rates based on the spectral radius.

The eigenvector associated with the spectral radius is highly oscillatory as the mesh is refined (recall this was true for the rowwise ordering also). An analysis similar to Garabedian's can be performed to find the convergence behavior for smooth initial data. To do this, we expand the real root of (3.24) at ω_{opt} about $\alpha_1=1$ using (2.14a) and (2.14b) to get the following equation which determines c_1 as a function of k_1 :

$$4c_1^2 - 5k_1c_1 + 6\pi^2 = 0\tag{3.27}$$

Choosing k_1 to maximize c_1 in (3.27) yields

$$k_1 = \frac{4}{5}\sqrt{6}\pi \approx 1.95959\pi\tag{3.28}$$

and

$$2c_1 = \sqrt{6}\pi \approx 2.44949\pi.\tag{3.29}$$

The corresponding values of ρ_{opt}^* and ω_{opt}^* are

$$\begin{aligned}\rho_{\text{opt}}^* &= 1 - 2.44949\pi h, \\ \omega_{\text{opt}}^* &= 2 - 1.95959\pi h.\end{aligned}\tag{3.30}$$

The values in (3.30) show that for smooth initial data this ordering is preferred over the rowwise ordering and Orderings 1 and 2. Note that the values in (3.26), based on the true spectral radius, lead to the opposite conclusion. However, the results of (3.26) are valid for nonsmooth initial data. Figure 3.11 shows the decay of $\|u\|_2$ for various initial data. For initial data obtained by discretizing the smooth data $u(x,y)=(x^2-x)(y^2-y)$, the observed decay is much closer to that predicted by (3.30), than to ρ^* .

Another ordering of the coloring in Figure 3.6b is R/G/B/O. This leads to a quartic equivalent to (2.10) with ξ and η interchanged. Hence, for a square grid with stepsize h in both the x and y

directions, ω_{opt} and ρ_{opt} for this ordering are also given by (2.21). Any of the 24 possible orderings associated with Figure 3.6b or the 24 orderings of Figure 3.6a can be easily proved (Adams and Jordan[1986]) to have the same eigenvalues as one of the three orderings (R/B/G/O, R/B/O/G, R/G/B/O) we have analyzed here. In addition, there is a third coloring of the grid that can be obtained by interchanging the rows and columns of Figure 3.6a. Any of the possible 24 orderings of this coloring also can be proved to be equivalent to one of the three we have analyzed. Hence, the 72 possible four-color orderings for this model problem can be grouped into two different equivalence classes that characterize the asymptotic convergence rate behavior.

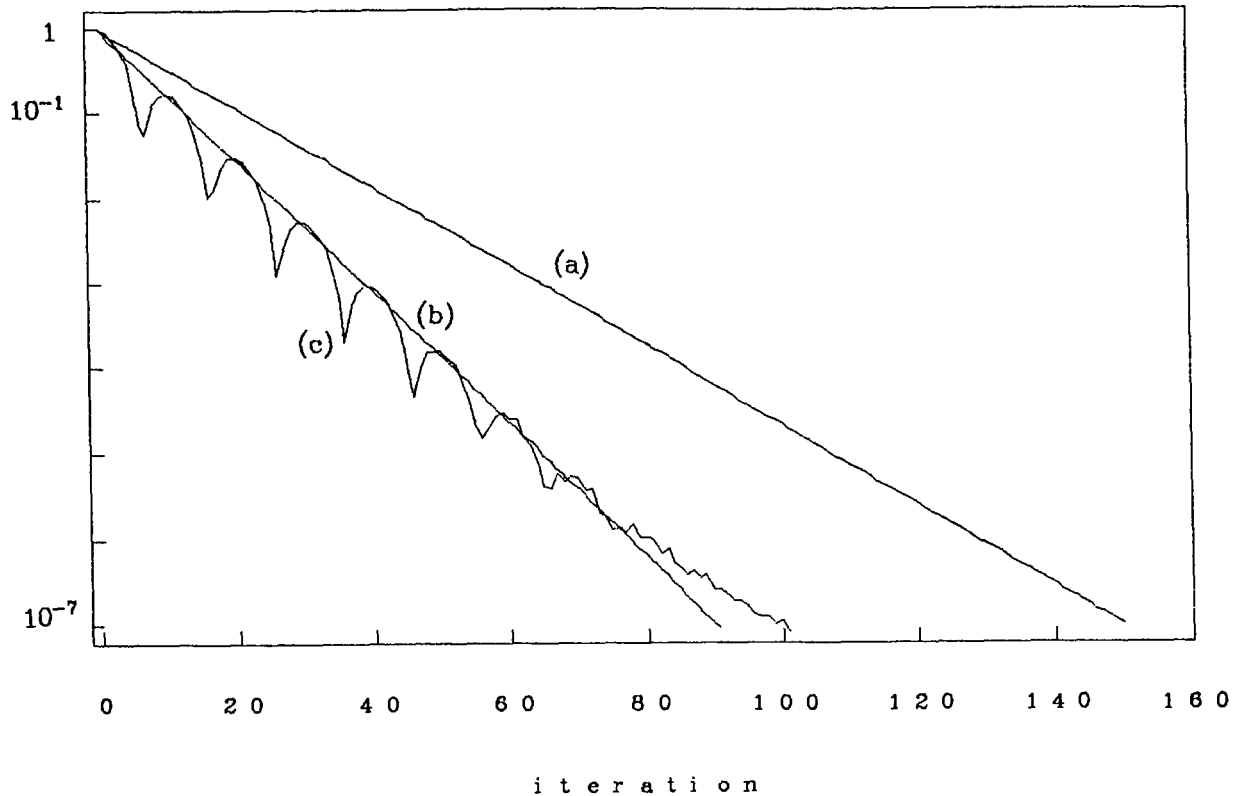


Figure 3.11. Convergence history (2-norm of error versus iteration number) for Ordering #3 with $h = 0.05$ and $\omega = 1.86$. Three choices of initial data are compared:

(a) An eigenvector corresponding to the spectral radius.

(b) An eigenvector corresponding to the largest nonspurious eigenvalue.

(c) $u_{jk}^0 = (x_j^2 - x_j)(y_k^2 - y_k)$.

Note that the realistic initial data (c) more closely matches (b) than (a).

4. A nine-point pseudo-SOR method.

We now consider a pseudo SOR method with the stencil in Figure 4.1,

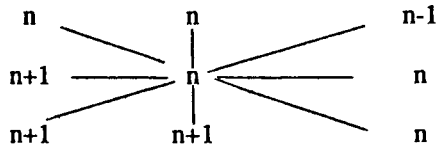


Figure 4.1. NR Modified Stencil in Variable n

and iteration

$$u_{jk}^{n+1} = (1-\omega) u_{jk}^n + \frac{\omega}{5} (u_{j,k-1}^{n+1} + u_{j-1,k}^{n+1} + u_{j+1,k}^n + u_{j,k+1}^n) \quad (4.1)$$

$$+ \frac{\omega}{20} (u_{j-1,k+1}^n + u_{j-1,k-1}^{n+1} + u_{j+1,k+1}^{n-1} + u_{j+1,k-1}^n)$$

which differs from (2.1) in the last two terms. This method can be analyzed using the techniques of Section 3. The earliest times for two iterations corresponding to Figure 4.1 are equal to those of Figure 3.2. That is, the iteration expressed in terms of the variable v is

$$u_{jk}^{v+1} = (1-\omega) u_{jk}^{v-1} + \frac{\omega}{5} (u_{j,k-1}^v + u_{j-1,k}^v + u_{j+1,k}^v + u_{j,k+1}^v) \quad (4.2)$$

$$+ \frac{\omega}{20} (u_{j-1,k+1}^{v-1} + u_{j-1,k-1}^{v-1} + u_{j+1,k+1}^{v-1} + u_{j+1,k-1}^{v-1}),$$

with the change of variables given by (3.3). It is interesting to note that the times in Figure 3.5 and the iteration in (4.2) are also obtained for a Red/Black ordering of the grid with the Red and Black stencils shown in Figure 4.2.

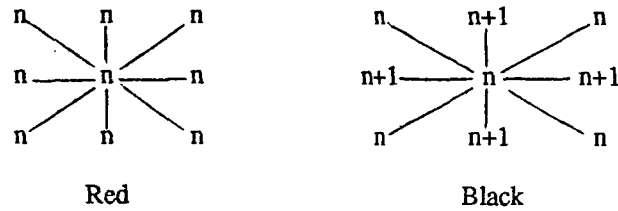


Figure 4.2. Red/Black 9-pt Modified Stencil in Variable n

Since two colors do not decouple a grid discretized with the 9-pt stencil, it is tempting to use old information for the Black to Black coupling as shown in Figure 4.2 to obtain a method suitable for parallel computers. This modification was considered by Kuo, Levy, and Musicus[1986] for a 9-pt stencil arising from a discretization of a PDE with a cross-derivative term. They show that the convergence rate of SOR for their problem to be $O(h)$ in the region where the lowest frequency dominates. We show by analyzing (4.2) that the use of only two colors is not sufficient for the 9-pt stencil arising from the Laplacian. In particular, we will show that the method converges whenever $0 < \omega < 5/3$, that the optimal omega occurs where the lowest and highest frequencies cross, and that the rate of convergence with the optimal omega is approximately $3\pi^2 h^2$ for small h as opposed to $1.79\pi h$ obtained in Section 3 for the true SOR method with Orderings #1 or #2.

We begin by observing that $u_{jk}^v = g^v \sin \xi x_j \sin \eta y_k$ is an eigenmode of (4.2). We substitute this into (4.2) to get

$$g^2 = (1-\omega) + \frac{2g\omega}{5} (\cos \xi h + \cos \eta h) + \frac{\omega}{5} \cos \xi h \cos \eta h, \quad (4.3)$$

where g^2 is the eigenvalue of the method in (4.1) or the Red/Black method depicted in Figure 4.2. The eigenvectors in variable n for the NR ordering (4.1) or the Red/Black ordering (Figure 4.2) are the same as the respective ones given in Section 3 for the 5-point stencil.

Equation (4.3) can be solved for g to get

$$g = \frac{\omega}{5} (\cos \xi h + \cos \eta h) \pm \sqrt{\frac{\omega^2}{25} (\cos \xi h + \cos \eta h)^2 + (1-\omega) + \frac{\omega}{5} \cos \xi h \cos \eta h}. \quad (4.4)$$

When $\omega=1$, the "pseudo Gauss-Siedel" method has amplification factor

$$g_{\pm}^2 = \left[\frac{\cos\xi h + \cos\eta h}{5} \pm \sqrt{\frac{1}{25}(\cos\xi h + \cos\eta h)^2 + \frac{1}{5}(\cos\xi h \cos\eta h)} \right]^2 \quad (4.5)$$

which is maximized when $\xi = \eta = \pi$. The maximum value is easily determined from (4.5) be $\cos^2\pi h$. This is identical to the spectral radius of Gauss-Siedel for the model problem with the 5-pt stencil. The methods, however, differ drastically when $\omega \neq 1$.

To determine the optimal ω , we must minimize the maximum modulus of g in (4.4). Two cases must be considered. First, assume the radical in (4.4) is negative. Then

$$|g|^2 = \omega \left(1 - \frac{1}{5} \cos\xi h \cos\eta h\right) - 1 \quad (4.6)$$

and for convergence, we require $|g|^2 < 1$ and hence

$$0 < \omega < \frac{2}{1 - \frac{1}{5} \cos\xi h \cos\eta h}. \quad (4.7)$$

As $h \rightarrow 0$, (4.7) shows that the method is divergent for $\omega > 5/3$. Also (4.6) shows that the value of $|g|^2$ is maximized when $\cos\xi h = -\cos\eta h$. This occurs when $\eta = N - \xi$ (low frequency in one direction and high frequency in the other) and this maximum is

$$|g|_{\max}^2 = \omega \left(1 + \frac{1}{5} \cos^2\pi h\right) - 1. \quad (4.8)$$

As $h \rightarrow 0$, $|g|_{\max}^2 \rightarrow \left|\frac{6}{5}\omega - 1\right|$.

Secondly, assume the radical in (4.4) is positive. Then, the maximum value of g occurs when $\xi = \eta = \pi$ and is

$$g_{\max}^2 = \frac{8}{25} \omega^2 \cos^2\pi h + (1 - \omega) + \frac{\omega}{5} \cos^2\pi h + \frac{4}{5} \omega \cos\pi h \sqrt{\frac{4}{25} \omega^2 \cos^2\pi h + (1 - \omega) + \frac{\omega}{5} \cos^2\pi h}. \quad (4.9)$$

It is interesting to note that the ω that minimizes (4.9) occurs when the radical is zero, and as $h \rightarrow 0$, $\omega \rightarrow 5/2$. That is, the method is divergent for the ω that minimizes g_{\max}^2 of (4.9) for the lowest frequency. Recall that the ω that is optimal for SOR for consistently ordered matrices corresponds to the

lowest frequency. For the pseudo SOR method, the optimal ω occurs where the modulus of the eigenvalues of the two frequencies $\eta=N-\xi$ and $\eta=\xi=\pi$ are equal. This ω is determined by equating (4.8) and (4.9) to get

$$\frac{16\omega^2\cos^2\pi h}{25} \left[\frac{\omega}{5}\cos^2\pi h + \omega - 1 \right] - 4(\omega-1)^2 = 0. \quad (4.10)$$

As $h \rightarrow 0$, $\omega \rightarrow 5/3$, so we look for a solution to (4.10) of the form

$$\omega(h) = \frac{5}{3} + c_1 h + c_2 h^2 + \dots \quad (4.11)$$

Substituting (4.11) into (4.10) and equating terms yields

$$c_1 = 0, \quad c_2 = -\frac{20}{9}\pi^2$$

and the corresponding values of the optimal ω and spectral radius of (4.1) are

$$\begin{aligned} \omega_{\text{opt}} &\approx \frac{5}{3} - \frac{20}{9}\pi^2 h^2 \\ \rho_{\text{opt}} &\approx 1 - 3\pi^2 h^2. \end{aligned} \quad (4.12)$$

Comparing (4.12) to $\cos^2\pi h \approx 1 - \pi^2 h^2$, the spectral radius of the pseudo Gauss Siedel method, shows that as $h \rightarrow 0$, this method with optimal ω is only three times faster than with $\omega=1$. This is not nearly as good as the true SOR methods discussed in Section 3, where the decay factor is $1 - O(h)$ for the optimal ω .

5. Comparison of point and line methods.

Let the system $Ax=b$ be blocked as

$$\begin{bmatrix} D_1 & -U_{12} & \dots & -U_{1m} \\ -L_{21} & D_2 & \dots & -U_{2m} \\ \cdot & -L_{32} & \dots & \cdot \\ \cdot & \cdot & \dots & \cdot \\ -L_{m1} & -L_{m2} & \dots & D_m \end{bmatrix} \begin{bmatrix} u_1 \\ u_2 \\ \cdot \\ \cdot \\ u_m \end{bmatrix} = \begin{bmatrix} b_1 \\ b_2 \\ \cdot \\ \cdot \\ b_m \end{bmatrix}. \quad (5.1)$$

The line Jacobi method is defined as

$$D_i u_i^{n+1} = \sum_{j<i} L_{ij} u_j^n + \sum_{j>i} U_{ij} u_j^n + b_i \quad (5.2)$$

and the line-SOR method as

$$D_i u_i^{n+1} = \omega \sum_{j<i} L_{ij} u_j^{n+1} + \omega \sum_{j>i} U_{ij} u_j^n + \omega b_i + (1-\omega) D_i u_i^n, \quad (5.3)$$

where u_i corresponds to the nodes in row i of the grid. The spectral radius of the Jacobi method for the 5-pt and 9-pt stencils can easily be found by separation of variables since $\sin \xi x_j \sin \eta y_k$ is an eigen-vector of iteration (5.2). These results are given in Figure 5.1.

Method	Spectral Radius
5-pt point	$\cos \pi h \approx 1 - \frac{1}{2} \pi^2 h^2$
5-pt line	$\frac{\cos \pi h}{2 - \cos \pi h} \approx 1 - \pi^2 h^2$
9-pt point	$\frac{4}{5} \cos \pi h + \frac{1}{5} \cos^2 \pi h \approx 1 - \frac{3}{5} \pi^2 h^2$
9-pt line	$\frac{\frac{2}{5} \cos \pi h + \frac{1}{5} \cos^2 \pi h}{1 - \frac{2}{5} \cos \pi h} \approx 1 - \pi^2 h^2$

Figure 5.1. Spectral Radius of Point and Line Jacobi Methods

The spectral radius of the line-SOR method for the 5-pt and 9-pt stencils can now be found using Young's theory for block-consistently ordered matrices. That is, if μ is the spectral radius of line-Jacobi then ω_{opt} and ρ_{opt} for line-SOR are given by

$$\omega_{\text{opt}} = \frac{2}{1 + \sqrt{1 - \mu^2}} \quad (5.4)$$

$$\rho_{\text{opt}} = \omega_{\text{opt}} - 1.$$

These SOR results are summarized in Figure 5.2 below where Garabedian's results for the 9-pt point methods are given in parenthesis.

Method	Ordering	Spectral Radius
5-pt point	Rowwise or Red/Black	$1-2\pi h$
5-pt line	Rowwise or Red/Black	$1-2\sqrt{2}\pi h$
9-pt point	Ordering #1	$1-1.79\pi h$ ($1-2.35\pi h$)
9-pt point	Ordering #2	$1-1.79\pi h$ ($1-2.35\pi h$)
9-pt point	Ordering #3	$1-1.60\pi h$ ($1-2.45\pi h$)
9-pt point	Rowwise	$1-1.79\pi h$ ($1-2.35\pi h$)
9-pt line	Rowwise or Red/Black	$1-2\sqrt{2}\pi h$

Figure 5.2. Spectral Radius for Point and Line SOR Methods

Figure 5.2 shows that, based on the actual spectral radius, the line methods converge faster than the point methods for both the 5 and 9 point stencils. The 9-pt line SOR method has the same convergence rate as the 5-pt line SOR method for small h ; whereas the 5-pt point SOR method with a consistent ordering can be expected to converge slightly faster than any of the 9-pt point SOR methods that we analyzed. However, the convergence rate that will be observed in practice with smooth initial data for the 9-pt point methods will be closer to Garabedian's results. That is, we can still expect the 9-pt line methods to converge slightly faster than the point methods, but now, the 9-pt point methods will converge faster than the 5-pt point method. This later fact is encouraging since the 9-point discretization is more accurate than the 5-point one.

6. Conclusions.

The SOR method with several orderings and a pseudo SOR method have been analyzed for the 9-point Laplacian. The Fourier analysis techniques proposed by LeVeque and Trefethen[1986] and separation of variables techniques were used to determine the eigenvalues and the eigenvectors of these methods.

We examined the SOR method for the 9-pt Laplacian using the natural rowwise ordering and several multicolor orderings. For all these orderings, we gave a quartic equation for the square root of the eigenvalues as a function of the frequencies and ω . The optimal ω was found by solving this quartic numerically for all our orderings. This ω was confirmed for some orderings by asymptotically solving the quartic corresponding to the lowest frequency for small h . The numerical results indicate that the lowest frequency determines the convergence rate, but so far we have not proved this.

Our results were confirmed by performing the SOR iteration with an initial guess corresponding to the eigenvector associated with the spectral radius. The observed rate of convergence matched that predicted by the theory to five decimal places. The SOR iteration was also performed by using a smooth initial guess, obtained by discretizing $(x-x^2)(y-y^2)$ for various stepsizes, h . In these cases, the observed convergence rate more closely resembled that predicted by Garabedian.

The results also show that different orderings of the same coloring can lead to different spectral radii: R/B/G/O and R/B/O/G for the coloring in 6b have spectral radii of $1-1.79\pi h$ and $1-1.60\pi h$ respectively. For smooth initial data, these two orderings also led to different effective spectral radii observed in practice; namely, $1-2.35\pi h$ and $1-2.45\pi h$, respectively. This information can be useful in selecting a coloring, an ordering, and appropriate initial data to use with multi-color SOR on parallel computers (Adams and Ortega[1982]).

An analysis of the pseudo SOR method showed that the optimal ω occurs when the high and low frequencies cross and that the corresponding spectral radius is only $1-3\pi^2 h^2$. This is inferior to both the 5-pt and 9-pt SOR methods we analyzed. In addition, for small h , the pseudo method only converges for $0 < \omega < 5/3$.

The 5-pt and 9-pt point and line SOR methods were compared for the model problem for small h . The line methods converge slightly faster than the point methods. The 9-pt line and 5-pt line methods have the same asymptotic rate of convergence, but the 5-pt point method with a consistent ordering was 1.12 times faster, based on the spectral radius, and 1.23 times slower, based on Garabedian's arguments, than the best 9-pt point method that we analyzed. Hence, for a smooth initial

guess, the 9-pt point methods can be expected to be more accurate and converge faster than the 5-pt point method.

Acknowledgement

The authors would like to thank Nick Trefethen for providing the initial stimulus for this work and for several valuable subsequent conversations. We also thank Elizabeth Ong for programming the SOR method with our orderings.

The authors wish to dedicate this paper, as a token of their highest esteem, to Professor Werner Rheinboldt on the occasion of his sixtieth birthday.

References

- Adams, L.M., Ortega, J.M. [1982]. "A Multi-Color SOR Method for Parallel Computation," *Proc. of the 1982 Intl. Conference on Parallel Processing*, IEEE Catalog No. 82CH1794-7, August, pp. 53-56.
- Adams, Loyce M., Jordan, Harry F. [1986]. "Is SOR Color-blind?", *Siam Journal on Scientific and Statistical Computing*, Vol. 7, No. 2, April, pp. 490-506.
- Forsythe, G., Wasow, W. [1960]. *Finite-Difference Methods For Partial Differential Equations*, John Wiley & Sons, Inc., New York, pp. 266.
- Frankel, S. [1950]. "Convergence Rates of Iterative Treatments of Partial Differential Equations," *Math. Comp.* 4, pp. 65-75.
- Garabedian, P. [1956]. "Estimation of the Relaxation Factor for Small Mesh Size," *Math. Comp.* 10, pp. 183-185.
- Kuo C., Levy B., Musicus B. [1986]. "A Local Relaxation Method for Solving Elliptic PDEs on Mesh-Connected Arrays," submitted to *Siam Journal on Scientific and Statistical Computing*.
- LeVeque R. and Trefethen L.N. [1986]. "Fourier Analysis of the SOR Iteration," submitted to *SIAM Journal of Numerical Analysis*.

Young, David M. [1950]. "Iterative Methods for Solving Partial Differential Equations of Elliptic Type," Doctoral thesis, Harvard University, Cambridge, Mass.

Young, David M. [1971]. *Iterative Solution of Large Linear Systems*, Academic Press, New York.

Standard Bibliographic Page

1. Report No. NASA CR-178212 ICASE Report No. 86-81		2. Government Accession No.		3. Recipient's Catalog No.	
4. Title and Subtitle ANALYSIS OF THE SOR ITERATION FOR THE 9-POINT LAPLACIAN				5. Report Date December 1986	
7. Author(s) Loyce Adams, Randy LeVeque, David Young				6. Performing Organization Code	
9. Performing Organization Name and Address Institute for Computer Applications in Science and Engineering Mail Stop 132C, NASA Langley Research Center Hampton, VA 23665-5225				8. Performing Organization Report No. 86-81	
12. Sponsoring Agency Name and Address National Aeronautics and Space Administration Washington, D.C. 20546				10. Work Unit No.	
				11. Contract or Grant No. NAS1-18107	
				13. Type of Report and Period Covered Contractor Report	
				14. Sponsoring Agency Code 505-90-21-01	
15. Supplementary Notes Langley Technical Monitor: Submitted to SIAM Journal on J. C. South Numerical Analysis Final Report					
16. Abstract The SOR iteration for solving linear systems of equations depends upon an overrelaxation factor ω . A theory for determining ω was given by Young [1950] for consistently ordered matrices. Here we determine the optimal ω for the 9-point stencil for the model problem of Laplace's equation on a square. We consider several orderings of the equations, including the natural rowwise and multicolor orderings, all of which lead to non-consistently ordered matrices, and find two equivalence classes of orderings with different convergence behavior and optimal ω 's. We compare our results for the natural rowwise ordering to those of Garabedian [1956] and explain why both results are, in a sense, correct, even though they differ. We also analyze a pseudo SOR method for the model problem and show that it is not as effective as the SOR methods. Finally, we compare the point SOR methods to known results for line SOR methods for this problem.					
17. Key Words (Suggested by Authors(s)) SOR (successive overrelaxation), multicolor orderings			18. Distribution Statement 64 - Numerical Analysis Unclassified - unlimited		
19. Security Classif.(of this report) Unclassified		20. Security Classif.(of this page) Unclassified		21. No. of Pages 40	22. Price A03